HHS Public Access

Author manuscript

Magn Reson Med. Author manuscript; available in PMC 2017 April 01.

Published in final edited form as:

Magn Reson Med. 2017 April ; 77(4): 1473–1484. doi:10.1002/mrm.26221.

Four-Dimensional Respiratory Motion-Resolved Whole Heart Coronary MR Angiography

Davide Piccini[1,2,*,†], **Li Feng**[3,†], **Gabriele Bonanno**[2], **Simone Coppo**[2], **Jérôme Yerly**[2,4], **Ruth P. Lim**[5], **Juerg Schwitter**[6], **Daniel K. Sodickson**[3], **Ricardo Otazo**[3], and **Matthias Stuber**[2,4]

[1]Advanced Clinical Imaging Technology, Siemens Healthcare, Lausanne, Switzerland [2]Department of Radiology, University Hospital and University of Lausanne, Lausanne, Switzerland [3]Center for Advanced Imaging Innovation and Research, and Bernard and Irene Schwartz Center for Biomedical Imaging, Department of Radiology, New York University School of Medicine, New York, New York, USA [4]Center for Biomedical Imaging, Lausanne, Switzerland [5]Department of Radiology, Austin Health and The University of Melbourne, Melbourne, Victoria, Australia [6]Division of Cardiology and Cardiac MR Center, University Hospital of Lausanne, Lausanne, Switzerland

Abstract

Purpose—Free-breathing whole-heart coronary MR angiography (MRA) commonly uses navigators to gate respiratory motion, resulting in lengthy and unpredictable acquisition times. Conversely, self-navigation has 100% scan efficiency, but requires motion correction over a broad range of respiratory displacements, which may introduce image artifacts. We propose replacing navigators and self-navigation with a respiratory motion-resolved reconstruction approach.

Methods—Using a respiratory signal extracted directly from the imaging data, individual signal-readouts are binned according to their respiratory states. The resultant series of undersampled images are reconstructed using an extradimensional golden-angle radial sparse parallel imaging (XD-GRASP) algorithm, which exploits sparsity along the respiratory dimension. Whole-heart coronary MRA was performed in 11 volunteers and four patients with the proposed methodology. Image quality was compared with that obtained with one-dimensional respiratory self-navigation.

Results—Respiratory-resolved reconstruction effectively suppressed respiratory motion artifacts. The quality score for XD-GRASP reconstructions was greater than or equal to self-navigation in 80/88 coronary segments, reaching diagnostic quality in 61/88 segments versus 41/88. Coronary sharpness and length were always superior for the respiratory-resolved datasets, reaching statistical significance ($P < 0.05$) in most cases.

Conclusion—XD-GRASP represents an attractive alternative for handling respiratory motion in free-breathing whole heart MRI and provides an effective alternative to self-navigation.

[*]Correspondence to: Davide Piccini Ph.D., Center for BioMedical Imaging, Centre Hospitalier Universitaire Vaudois, Rue de Bugnon 46, BH 7.84, 1011 Lausanne, Switzerland. piccinidavide@gmail.com; Twitter: @CVMR_Lausanne.
[†]Davide Piccini and Li Feng contributed equally to this study.

SUPPORTING INFORMATION

Additional Supporting Information may be found in the online version of this article.

Keywords

coronary MRA; free breathing; sparse reconstruction; compressed sensing; motion correction; self-navigation

INTRODUCTION

Coronary MR angiography (MRA) has improved substantially over the past two decades, showing promising results in relatively large patient cohorts (1–4). However, it still remains mostly confined to research use at a small number of experienced academic MR centers. The main shortcoming of coronary MRA is its vulnerability to motion-induced artifacts, which is linked with time-inefficient data collection. Conventional acquisitions are electrocardiogram-triggered to short time windows (~50–100 ms) of relative coronary quiescence (e.g., mid-diastole), and a large number of cardiac cycles is needed for sufficient high-resolution volumetric coverage. Consequently, free-breathing acquisitions are mandatory, but they necessitate sophisticated respiratory motion compensation approaches.

Navigator techniques (5–8), which identify the position of the right hemidiaphragm, typically gate data collection to a small acceptance window during end-expiration only. The drawbacks of these techniques include low scan efficiency, unpredictable scan times, sensitivity to respiratory drift, and the need for meticulous scan planning. Conversely, self-navigated techniques (9–14) that directly extract a respiratory motion signal from the imaging data to perform respiratory motion correction, operate with 100% scan efficiency, have highly predictable scan duration, and improved ease-of-use. Such techniques have been extensively tested in both volunteer (10,15,16) and patient (14,17) cohorts in single-center studies. However, self-navigation still suffers from limitations related to the motion model employed for correction (e.g., one-dimensional [1D], three-dimensional [3D], affine, etc.) (18), may not be sufficiently accurate for large-scale respiratory motion, and may be affected by artifacts originating from static anatomy after motion correction.

Several 3D self-navigation approaches have been proposed recently to subdivide the whole heart coronary dataset into subsets of volumes, each corresponding to a particular respiratory position or state (12,13,19,20). Because the quality of these imaging volumes is generally low due to the inevitable undersampling artifacts, all such methods propose to exploit these subsets uniquely for image registration, while the final reconstructed dataset is composed of all acquired k-space lines after motion correction. In this context, it has to be mentioned that the registration of undersampled volumes is a nontrivial problem, due, among other technical issues, to the artifact level connected to the undersampling. However, with the introduction of sparse reconstruction techniques, which exploit correlations between images in the series to reduce the number of k-space points required to reconstruct each individual image (21,22), the image quality of such subsets may potentially be enhanced such that image registration and corrected reconstruction are no longer be needed.

Recently, a novel image reconstruction framework known as extradimensional golden-angle radial sparse parallel (XD-GRASP) MRI was proposed, which combines the acceleration capabilities of reduced k-space sampling and sparse reconstruction with the self-navigation

properties of a hybrid radial and Cartesian (stack-of-stars) sampling scheme to reconstruct additional motion dimensions for dynamic liver imaging and cine cardiac imaging (23). 3D whole heart coronary MRA is a static rather than dynamic acquisition, but it can be an ideal extension for XD-GRASP, because the data acquired during free-breathing can be sorted and binned into multiple respiratory phases. This generates a fourth dimension, which represents the respiratory motion. As in the original XD-GRASP implementation, the new respiratory dimension can be regarded as an additional temporal correlation that can be exploited using a sparsity-based approach to reconstruct a four-dimensional (4D) dataset (3D + respiratory dimension). Nevertheless, to extend this approach and achieve the whole-heart coverage and high isotropic spatial resolution needed for free-breathing coronary imaging, a recently proposed (24) 3D golden angle radial sampling scheme was used. This sampling scheme not only enables the flexible a posteriori combination of k-space segments needed for the respiratory binning, it also provides additional incoherence when compared with the original XD-GRASP implementation.

We therefore hypothesize that such sparse reconstruction algorithms can be exploited to reconstruct respiratory motion-resolved 3D images of the heart without the need for breath-holding, navigators, self-navigated respiratory correction, or complex 3D motion correction.

METHODS

A general schematic representation of the acquisition and reconstruction pipeline is shown in Figure 1. Details about each step of the pipeline are provided in the sections below.

Data Acquisition

Written informed consent was obtained from all participants for this Institutional Review Board–approved study. Volunteer and patient data acquisitions were performed using a prototype segmented 3D radial trajectory (24). Such a trajectory is subjected to a golden angle rotation about the *z*-axis at each heartbeat, such that each acquired segment is intrinsically positioned within the largest k-space void left by the prior segments. Additionally, a readout with consistent superior–inferior (SI) orientation at the beginning of each segment can be used for either respiratory self-navigation (10) or respiratory data binning (25). Because of the unique golden angle rotational arrangement of the readouts, it is possible to retrospectively sort (i.e., bin) all segments according to the respiratory phases (motion states) at which they were acquired. This results in distinct pseudo-uniform 3D k-space coverage for each respiratory bin.

Free-breathing whole heart coronary MRA was performed in 11 healthy adult volunteers (male, n = 9; female, n = 2; mean age, 29 ± 4 y [range, 26–34 y]) and, as a first proof of principle, in four patients (male, n = 3; female, n = 1; mean age, 64 ± 7 y [range, 54–72 y]; sinus rhythm range 55–92 beats per minute) with established coronary artery disease. The acquisition was performed using electrocardiogram triggering on a 1.5T clinical MRI scanner (MAGNETOM Aera; Siemens Healthcare, Erlangen, Germany) with a total of 30 receiver coil elements. For the volunteer group, the acquisition window (~80–100 ms, ~25–32 k-space lines per cardiac cycle) was placed in mid-diastole and adapted to the individual subject's heart rate using visual inspection of a four-chamber cine dataset at high temporal

resolution while the scan was performed during approximately 400 heartbeats. For the patient group, the acquisition window was adapted to a shorter cardiac rest phase (~40–60 ms/12–20 k-space lines per cardiac cycle), which was compensated for by an increased number of heartbeats (~600). The protocol parameters of the 3D radial, non–slice-selective, T_2-prepared (echo time T_2 prep = 40 ms), fat-saturated, balanced steady state free precession imaging sequence included: repetition time = 3.1 ms; echo time = 1.56 ms; field of view = 220 mm^3, matrix = 192×192×192; voxel size = 1.15 mm^3; RF excitation angle = 90°; and receiver bandwidth = 898 Hz/Pixel. The total amount of k-space lines acquired in each case was approximately 12,000 for a total acquisition time of 7.0 ± 1.3 min.

Respiratory Motion Extraction

A recently described technique (25) that exploits signal amplitude variations from the center of k-space (KCA) (26) was adopted to extract respiratory-induced motion from all SI-oriented readouts. Because such variations have different contributions in each detector coil, the respiratory motion detection procedure (Fig. 2) was repeated for all coil elements individually. Subsequently, independent component analysis (27) was performed on the KCA signals from all coils to extract independent signal components. The signal component with maximum amplitude, within the bandwidth of the expected respiratory frequency (28), was used for respiratory binning.

Data Sorting

Figure 3a illustrates the data sorting procedure prior to XD-GRASP reconstruction. The whole heart coronary MRA data, acquired using the 3D radial trajectory, were subdivided into n subsampled 3D k-space datasets that originate from n different respiratory states. The number of k-space lines grouped in each individual state was the same. According to the golden angle acquisition scheme, nearly uniform coverage of k-space is ensured for each bin and distinct sampling patterns among those bins are automatically obtained so that temporal incoherence and sparsity can be exploited in the iterative reconstruction. For the current study, four and six respiratory phases were used for data binning (Fig. 3b,c). Although a six-phase subdivision of the breathing pattern leads to narrower and more sparsely populated bins (12,13), a four-phase subdivision leads to wider bins that are more densely populated. Both four- and six-phase XD-GRASP reconstructions were performed to investigate the effects of bin width on image quality.

According to prior experience (23), the regularization parameters of the XD-GRASP reconstruction were empirically optimized for four- and six-phase XD-GRASP on two representative training datasets by two coronary MRA experts (D.P. and M.S., with 7 and 20 years of experience in coronary MRA, respectively) blinded to the reconstruction parameters. Specifically, a range of values (0.005–0.1) of the regularization parameter were tested and compared visually. The values that generated the best image quality and coronary delineation were selected separately for the four- and six-phase XD-GRASP reconstructions.

Because the binning process is driven by the amount of data contained in each bin, the bin widths are not constant. Consequently, the amount of motion included in each bin is also variable within the same subject. The relative amount of motion included in each bin or

respiratory phase for the two binning approaches (four- and six-phase) was measured as the percentage width of each bin relative to the entire respiratory excursion of a subject, and these bin widths (expressed in %) were then averaged across all subjects. All values were reported as the mean ± standard deviation.

Image Reconstruction

XD-GRASP reconstruction was performed on all binned coronary datasets by solving the following optimization problem that enforces joint multicoil sparsity on the extradimensional dataset using a sparsifying transform along the new respiratory dimension

$$d=\underset{d}{\operatorname{argmin}}\|F\cdot C\cdot d-m\|_2^2+\lambda\|S\cdot d\|_1, \quad [1]$$

where ***F*** is the nonuniform fast Fourier transform (NUFFT) operator defined for the 3D golden angle radial sampling pattern; ***C*** represents the multiple-element coil sensitivity maps with dimensionality of the *x*–*y*–*z*– coil (where *x*, *y*, and *z* represent the three spatial dimensions); ***d*** is the respiratory motion-resolved image series with dimensions *x*–*y*–*z*–*t*; and ***m*** represents the corresponding multicoil radial k-space data, which are sorted according to the respiratory state with dimension *x*–*y*–*z*–*t*–coil. The sparsifying transform ***S*** is the first-order difference between respiratory states and the minimization of its l_1 norm is commonly known as total variation minimization. This approach is well suited for applications where the image or volume is piecewise constant, and it has performed well when compared with other recently proposed sparsifying transforms (29). Finally, λ is the regularization parameter that weighs the contribution of the joint multicoil sparse regularization with respect to data consistency. Image reconstruction was implemented as described in Feng et al. (23), and the most end-expiratory volume was chosen for image analysis.

For comparison, each coronary dataset was also reconstructed using 1D respiratory self-navigation as described by Piccini et al. (14). For respiratory self-navigation, respiratory motion was extracted by cross-correlating the automatically segmented blood pool on the 1D FFT of an end-expiratory reference SI readout (reference SI projection) (15) to all other SI projections. The resulting 1D SI displacement was then used for correcting each data segment before the gridding operation by directly applying a phase shift to all k-space readouts and was adapted for the polar orientation of each signal readout. Image reconstruction was performed using a 3D regridding algorithm that makes use of a uniform density compensation function and a Kaiser–Bessel window. The multicoil 3D images were then combined using coil sensitivity maps estimated using the adaptive combination approach described in Walsh et al. (30). A detailed description of the segmentation and cross-correlation algorithms can be found in Piccini et al. (14).

All reconstructions were performed using a server equipped with two 16-core Opteron CPUs, 256 Gb RAM, and two 6-Gb NVIDIA graphics processing unit (GPU) cards. The NUFFT operation was implemented using parallel computing on GPUs (31), and the main reconstruction program was implemented in MATLAB 2012b (MathWorks, Natick, Massachusetts, USA).

Volunteer Study

All 1D respiratory self-navigated and end-expiratory phases of XD-GRASP reconstructed volunteer datasets were pooled, anonymized, and randomized prior to image analysis.

Quantitative Assessment—To objectively determine the quality of vessel depiction, the proximal and mid-segments of both the right coronary artery (RCA) and the left anterior descending coronary artery (LAD) as well as the left main stem (LM) and the proximal left circumflex coronary artery (LCX) were identified on all datasets, as described by Austen et al. (32). The percentage vessel sharpness was computed for each of these segments as described by Etienne et al. (33). The total visible vessel lengths were also measured for both the left coronary system (sum of LM and LAD) and the RCA.

Image Quality Assessment—On all datasets, the image quality of the entire LM; the proximal, mid-, and distal segments of the LAD and RCA; and the proximal LCX were graded on a 5-point scale similar to that described by McConnell et al (34). The two aforementioned experts performed this grading (image quality grading) using consensus reading (3). The scale classified the definition of the vessel borders as follows: 0 = not visible, 1 = markedly blurred, 2 = moderately blurred, 3 = mildly blurred and, 4 = sharply defined. The average values of the quality grading were recorded, as were the number of equal or higher scores in either of the two techniques.

Diagnostic Quality Assessment—The diagnostic quality and visibility of each segment of LM, LAD, RCA, and proximal LCX were graded for all coronary datasets on a 3-point scale (diagnostic quality grading) by an experienced cardiovascular MR radiologist (R.P.L., with 10 years of experience), blinded to the type of reconstruction. The scale used was as follows: 0 = not visible, 1 = visible but nondiagnostic, and 2 = diagnostic.

Statistical Analysis—Statistical comparisons for the vessel sharpness and length were performed with a paired two-tailed Student *t* test in Microsoft Excel (Microsoft, Redmond, Washington, USA) and $P < 0.05$ was considered statistically significant. For quality grading and diagnostic grading, a nonparametric paired two-tailed Wilcoxon signed-rank test was used to compare the scores on a per-vessel segment basis, as well as all scores for all segments of all patients considered together. Finally, a McNemar's statistical test was used to assess statistical significance for the number of coronary segments that were graded as diagnostic with the three reconstructions. Bonferroni correction was applied where needed to correct for the multiple comparisons.

Initial Data Collection in Patients

Patient data were reconstructed using the four-phase XD-GRASP reconstruction, and because of the small sample size, the results were only visually compared with 1D respiratory self-navigation. Identification of the location of coronary stenoses on MRI was also visually compared with the findings from the gold standard X-ray coronary angiography.

RESULTS

Data Sorting

A four-phase XD-GRASP reconstruction was found to be sufficient for resolving respiratory motion, and a regularization parameter of $\lambda = 0.02$ led to an optimal balance between removal of undersampling artifacts and reconstructed image quality. A six-phase XD-GRASP reconstruction achieved similar performance with a higher regularization parameter ($\lambda = 0.05$) to account for the higher degree of undersampling. The relative amount of respiratory displacement for each of the bins was the smallest for the end-expiratory phase, with 14.6% ± 4.8% and 8.2% ± 2.8% of the total motion for the four-phase and six-phase reconstruction, respectively. The phases with largest respiratory displacement were measured around end-inspiration at 35.3% ± 8.0% and 27.1% ± 7.4% for four-phase and six-phase XD-GRASP, respectively. Figure 4 shows images from one representative volunteer in whom conventional gridding reconstructions with sensitivity-weighted multicoil combination for each respiratory phase, after binning, were visually compared with those obtained from four-phase XD-GRASP. As evidenced by a gradual shift of both the heart and the liver in these images, respiratory motion can be resolved and accounted for by sorting the data into different motion states, whereas undersampling artifacts are efficiently removed with XD-GRASP reconstruction. Image quality of the motion states improved considerably using XD-GRASP, whereas the image registration step was no longer needed.

Image Reconstruction

The whole heart coronary MRA acquisitions and reconstructions were successful for all volunteer and patient scans. The average reconstruction time for XD-GRASP was 35.1 4.5 min and 58.2 ± 5.6 min for four-phase and six-phase XD-GRASP, respectively. By comparison, the 1D respiratory self-navigation inline reconstruction on the scanner lasted <2 min.

Volunteer Study

An overview of the numerical results of image quality grading, vessel sharpness, and length measurements is reported in Table 1.

Quantitative Assessment—Greater or equal vessel sharpness with respect to 1D respiratory self-navigation was obtained in 56/66 and 49/66 coronary segments, and the total visible vessel length was superior or equal in 17/22 and 15/22 evaluated coronary arteries for the four- and six-phase XD-GRASP reconstructions, respectively. The average vessel sharpness and length were superior for both XD-GRASP reconstructions with respect to 1D respiratory self-navigation. Four-phase XD-GRASP vessel sharpness was significantly superior to 1D respiratory self-navigation for the LM ($P < 0.003$), proximal, and mid-LAD ($P < 0.04$ and $P < 0.007$) and mid-RCA ($P < 0.008$). Visualized length of LM LAD ($P < 0.05$) was also improved. In addition, significantly superior results for the six-phase XD-GRASP reconstruction were achieved for the sharpness values of the mid-RCA ($P < 0.005$) compared with 1D respiratory self-navigation. Figure 5 shows multiplanar reformats of the coronary arteries from one representative volunteer: although 1D respiratory self-navigation

already led to adequate image quality (Fig. 5a), there was a clear improvement in sharpness and visible vessel length in both the four-phase and six-phase XD-GRASP reconstructions.

Image Quality Assessment—In the vast majority of cases, the respiratory-resolved XD-GRASP reconstruction achieved equal or improved image quality grades relative to 1D respiratory self-navigation. In particular, the quality grade was greater or equal in 76/88 and in 80/88 coronary segments for the four- and six-phase XD-GRASP reconstructions, respectively. The average grade of the qualitative assessment was superior for both XD-GRASP reconstructions, except for the quality grade of the proximal LCX, which was very similar to that of 1D respiratory self-navigation. The paired two-tailed Wilcoxon signed-rank test showed statistical significance for the improvements in the image quality grades of all coronary segments considered together for both four-phase XD-GRASP reconstruction ($P < 0.0001$) and six-phase XD-GRASP reconstruction ($P < 0.0001$) compared with 1D respiratory self-navigation. There was no statistically significant difference ($P = 0.06$) between the two XD-GRASP reconstructions. When looking at the per segment analysis, statistical significance was reached for the mid-LAD for the four-phase XD-GRASP and for the mid-LAD, mid-RCA, and distal RCA for six-phase XD-GRASP (Table 1).

Diagnostic Quality Assessment—The results related to the diagnostic grading are reported in Table 2. Overall, the ratio of coronary segments labeled as diagnostic increased from 41/88 for 1D respiratory self-navigation to 61/88 and 56/88 for the four- and six-phase XD-GRASP reconstructions, respectively. Conversely, the total ratio of nonvisible segments decreased from 5/88 with 1D respiratory-self navigation to 1/88 with both four-and six-phase XD-GRASP reconstructions.

The diagnostic grades obtained for the four-phase XD-GRASP reconstructions were higher or equal to those of 1D respiratory self-navigation in 87/88 coronary segments, whereas this ratio was 85/88 for six-phase XD-GRASP. On average, the diagnostic grades for the XD-GRASP reconstructions were always higher than those obtained with 1D respiratory self-navigation, with the only exception being the proximal LCX. The four-phase XD-GRASP reconstruction reached 100% diagnostic quality for LM, proximal LAD, and proximal RCA. Full diagnostic quality was also reached with the six-phase reconstruction for LM and proximal RCA.

The paired two-tailed Wilcoxon signed-rank test showed statistical significance for the improvements in the diagnostic quality grades of all coronary segments considered together for both four-phase XD-GRASP reconstruction ($P < 0.0001$) and six-phase XD-GRASP reconstruction ($P < 0.0005$) compared with 1D respiratory self-navigation. The McNemar's statistical test showed that the increase in the number of diagnostic coronary segments was significant for both four-phase ($P < 0.0001$) and six-phase ($P < 0.003$) reconstructions with respect to 1D respiratory self-navigation. Also in this case, a comparison between the four-phase and six-phase approach did not yield statistically significant results.

A volunteer dataset in which 1D respiratory self-navigation did not achieve diagnostic quality is shown in Figure 6. Although there was a visual improvement with respect to the uncorrected reconstruction (where gridding of all k-space lines was performed without any

respiratory motion correction), the coronal view showed substantial residual blurring, and only the proximal segments of LAD and LCX were visible. Even though a long contiguous segment of the RCA was displayed, diagnostic quality was not reached for the more distal segments. By contrast, using XD-GRASP reconstruction, sharp and well-defined borders of coronary, myocardial, and hepatic structures can be appreciated. Coronary segments that were graded as visible but non-diagnostic on the 1D respiratory self-navigation were considered diagnostic after XD-GRASP reconstruction.

Initial Findings in Patients

All datasets were successfully reconstructed in this initial and small patient cohort. All patients had at least two-vessel coronary artery disease in the proximal or mid-segments as diagnosed by X-ray coronary angiography. In three of the four patients, one or more coronary stenoses were successfully visualized by way of MR. The image quality of the fourth patient was not sufficient to confirm stenoses in the mid- and distal coronary segments. Importantly, the regularization term of the four-phase XD-GRASP reconstruction did not affect the depiction of stenosis, and the vessels appeared sharper than in the reformats from 1D respiratory self-navigation. Example reformats from one coronary artery disease patient are shown in Figure 7; both 1D respiratory self-navigation and four-phase XD-GRASP reconstruction are shown in comparison to the gold standard X-ray coronary angiogram. A significant stenosis of the proximal LAD was well visualized in both the self-navigated and the XD-GRASP reconstruction.

DISCUSSION

XD-GRASP has been introduced previously as a sparse iterative reconstruction technique that can be exploited for motion suppression in dynamic MRI using a stack-of-stars sampling scheme (23). In the present study, the XD-GRASP framework was extended for free-breathing, 3D whole heart coronary MRA. For this purpose, it was combined with a 3D golden-angle radial trajectory that enables not only whole heart coverage at high isotropic spatial resolution but also a flexible a posteriori combination of k-space segments that are regrouped into pseudo-uniform phases or bins.

Specifically, we tested the hypothesis that this approach can be leveraged to reconstruct respiratory motion-resolved 3D images of the heart without the need for navigators, self-navigated respiratory correction, or tailored models for 3D motion correction. A respiratory signal is extracted directly from the imaging data and is used only for sorting the acquired data into multiple respiratory states. Although conventional gridding reconstruction of the individual bins may provide motion-resolved images, the considerable degree of under-sampling would inevitably lead to noise and streaking artifacts. However, the correlation along the new respiratory dimension is well suited for reconstruction using the XD-GRASP framework. With this approach, image registration of low-quality sub-images can be avoided, as the respiratory dimension is used to create a sparse time domain that can be exploited to enhance the image quality of each individual respiratory bin. Although the end-expiratory 3D volume of the XD-GRASP reconstruction was selected for coronary artery visualization in our study, it should be noted that the reconstructed motion-resolved datasets

contain abundant anatomic information across the whole respiratory cycle, which may be exploited further (Supporting Video 1).

This approach was tested in a group of healthy adult volunteers and preliminarily in a small number of patients with coronary artery disease and was compared with 1D respiratory self-navigation. In this context, it is important to emphasize that the exact same acquired data were used, yet the reconstruction pathway was different. The results show that vessel conspicuity and vessel length were superior with the proposed methodology. The image quality assessment was used to identify the overall improvements in image quality and was performed by the first and last authors of the manuscript, who have the most experience in coronary MRA. Although this might be a potential source of bias, the results were fully confirmed by the diagnostic quality assessment, which was performed by an independent reviewer and answered the question of whether diagnostic quality was obtained with each technique. Furthermore, initial patient data also demonstrated considerable promise for improved delineation of proximal coronary segments.

Because conventional whole heart coronary MRA is commonly performed with end-expiratory navigator gating that suffers from variable scan efficiency and unpredictable scanning times, several groups have proposed the acquisition of data during the entire respiratory cycle, together with aggressive motion correction to obtain reduced and predictable scan times (9–11). In most cases, respiratory motion is retrospectively corrected using registration algorithms (12,13,18,35). However, the motion correction performed using specific motion models (11,13,36,37) remains an approximation of the real respiratory-induced motion of the heart. Hypothetically, this limitation promises to be intrinsically addressed using the XD-GRASP methodology, because neither motion models nor registration algorithms are required. Nevertheless, a direct comparison between the proposed motion-resolved reconstruction approach and established techniques based on navigator gating will be required to test this hypothesis. However, the 1D self-navigation technique has already been compared with the standard navigator-gated technique in volunteers (10), and similar image quality was obtained. For this reason, and because of scan time constraints, a direct comparison between the XD-GRASP technique and a standard navigator-gated technique was not added to the present study.

An important aspect also relates to the tradeoff between the number of reconstructed respiratory phases and the residual, intra-bin, sparsity artifacts. Here, XD-GRASP reconstruction was performed with both four and six respiratory phases. Although the use of a larger number of respiratory phases might be expected to better resolve respiratory motion and reduce blurring, a higher number of phases is also associated with increased degrees of undersampling in each of them. The results suggest that, for our healthy volunteer cohort, both four-and six-phase XD-GRASP reconstructions are very similar in performance. Ideally, the number of reconstructed respiratory phases could be tailored to the specific breathing pattern of each subject—choosing, for example, less phases for more regular breathers, where the overall respiratory displacement is relatively small, and more phases for irregular breathers, where the total respiratory amplitude may be larger (38). Although the results obtained in the initial patient cohort seem to confirm that a four-phase reconstruction might be sufficient also for this population, the number of subjects is too small and the link

between respiratory drift or irregular breathing and an optimal reconstruction yet remains to be ascertained. Further analyses on a larger patient population would be useful to investigate the relationship between the different breathing patterns and the optimal number of reconstructed phases.

Although sparse reconstruction techniques have been applied previously for whole heart coronary MRA (20,39–43), most of the implementations aim at reducing the acquisition time by exploiting spatial correlations. XD-GRASP, on the other hand, sorts the acquired data into an additional respiratory dimension and exploits sparsity in this new dynamic dimension. The high correlation in this respiratory dimension enables improved performance in XD-GRASP reconstruction compared with conventional sparse reconstructions exploiting spatial correlation only.

The golden-angle arrangement of the 3D radial phyllotaxis trajectory intrinsically facilitates the extraction of the respiratory motion signal directly from the image data (since all readouts cross the k-space center) and provides flexibility in data sorting (since quasi-uniform spatial sampling over time—and therefore in all respiratory bins—is facilitated). Simultaneously, the golden angle rotation ensures a certain level of incoherence along the new respiratory dimension, which is required for XD-GRASP reconstruction (i.e., the data are sufficiently distinct in different motion states, since the same k-space profile is never acquired twice).

In electrocardiogram-triggered whole heart coronary MRA, data acquisition is typically performed during a short acquisition window in diastole. However, 4D cardiac and respiratory motion-resolved whole heart coronary MRA approaches have been proposed recently (44,45) that advocate continuous data acquisition through the entire cardiac cycle. Coronary artery images can be reconstructed at different cardiac phases, and additional information on 3D cardiac function can be extracted. The extension of these 4D approaches with XD-GRASP seems straightforward, and it would enable simultaneous exploitation of correlations in both cardiac and respiratory dimensions, thus leading to 5D cardiac MRI.

Two limitations of our initial proof-of-concept implementation include: 1) lengthy reconstruction times due to the iterative reconstruction process, which requires the computation of one forward and one inverse 3D NUFFT for each respiratory phase and coil per iteration, and 2) substantial memory requirements to respond to the computational needs associated with large, high-resolution 3D datasets. However, with continued progress in computer hardware and software, this is not likely to be a future roadblock. Although this study had a strong focus on coronary MRA with most stringent boundary conditions because of the small and tortuous nature of the vessels, the XD-GRASP approach will likely benefit other 3D cardiac imaging techniques such as delayed hyperenhancement studies and T1 and T2 mapping. Finally, XD-GRASP may potentially be combined with methods that simultaneously exploit the spatial sparsity of the images. Based on earlier numerical simulations (29), only a moderate improvement in image quality is expected and an increasing degree of freedom for optimization of the regularization weights will have to be considered.

CONCLUSION

A powerful alternative to navigators or self-navigation for handling respiratory motion in 3D whole heart coronary MRA has been proposed. The XD-GRASP framework can be exploited to reconstruct respiratory motion-resolved 3D images of the heart without the need for breath-holding, navigators, self-navigated respiratory motion correction, or complex 3D correction schemes.

Instead of discarding data segments from inconsistent respiratory phases or enforcing motion models for motion correction that are inevitably imperfect, XD-GRASP makes constructive use of all respiratory phases to improve image quality and achieves superior image quality compared with 1D respiratory self-navigation. A 3D radial phyllotaxis trajectory and XD-GRASP reconstruction provide a synergistic combination that ultimately may lead coronary MRA closer to clinical practice.

Supplementary Material

Refer to Web version on PubMed Central for supplementary material.

Acknowledgments

We would like to thank Dr. Florian Knoll from NYU School of Medicine for his support with the GPU implementation of 3D NUFFT.

Grant sponsor: Center for Advanced Imaging Innovation and Research (CAI2R, www.cai2r.net), a NIBIB Biomedical Technology Resource Center; Grant number: P41 EB017183; Grant sponsor: Swiss National Science Foundation; Grant number: 143923.

References

1. Kato S, Kitagawa K, Ishida N, et al. Assessment of coronary artery disease using magnetic resonance coronary angiography: a national multicenter trial. J Am Coll Cardiol. 2010; 56:983–991. [PubMed: 20828652]
2. Sakuma H. Coronary CT versus MR angiography: the role of MR angiography. Radiology. 2011; 258:340–349. [PubMed: 21273518]
3. Kim WY, Danias PG, Stuber M, et al. Coronary magnetic resonance angiography for the detection of coronary stenoses. N Engl J Med. 2001; 345:1863–1869. [PubMed: 11756576]
4. Hamdan A, Asbach P, Wellnhofer E, Klein C, Gebker R, Kelle S, Kilian H, Huppertz A, Fleck E. A prospective study for comparison of MR and CT imaging for detection of coronary artery stenosis. JACC Cardiovasc Imaging. 2011; 4:50–61. [PubMed: 21232704]
5. Ehman RL, McNamara MT, Pallack M, Hricak H, Higgins CB. Magnetic resonance imaging with respiratory gating: techniques and advantages. Am J Roentgenol. 1984; 143:1175–1182. [PubMed: 6333787]
6. Wang Y, Rossman PJ, Grimm RC, Riederer SJ, Ehman RL. Navigatorecho-based real-time respiratory gating and triggering for reduction of respiration effects in three-dimensional coronary MR angiography. Radiology. 1996; 198:55–60. [PubMed: 8539406]
7. Danias PG, McConnell MV, Khasgiwala VC, Chuang ML, Edelman RR, Manning WJ. Prospective navigator correction of image position for coronary MR angiography. Radiology. 1997; 203:733–736. [PubMed: 9169696]
8. Stuber M, Botnar RM, Danias PG, Sodickson DK, Kissinger KV, Van Cauteren M, De Becker J, Manning WJ. Double-oblique free-breathing high resolution three-dimensional coronary magnetic resonance angiography. J Am Coll Cardiol. 1999; 34:524–531. [PubMed: 10440168]

9. Stehning C, Bornert P, Nehrke K, Eggers H, Stuber M. Free-breathing whole-heart coronary MRA with 3D radial SSFP and self-navigated image reconstruction. Magn Reson Med. 2005; 54:476–480. [PubMed: 16032682]
10. Piccini D, Littmann A, Nielles-Vallespin S, Zenge MO. Respiratory self-navigation for whole-heart bright-blood coronary MRI: methods for robust isolation and automatic segmentation of the blood pool. Magn Reson Med. 2012; 68:571–579. [PubMed: 22213169]
11. Henningsson M, Koken P, Stehning C, Razavi R, Prieto C, Botnar RM. Whole-heart coronary MR angiography with 2D self-navigated image reconstruction. Magn Reson Med. 2012; 67:437–445. [PubMed: 21656563]
12. Bhat H, Ge L, Nielles-Vallespin S, Zuehlsdorff S, Li D. 3D radial sampling and 3D affine transform-based respiratory motion correction technique for free-breathing whole-heart coronary MRA with 100% imaging efficiency. Magn Reson Med. 2011; 65:1269–1277. [PubMed: 21500255]
13. Pang J, Bhat H, Sharif B, Fan Z, Thomson LE, Labounty T, Friedman JD, Min J, Berman DS, Li D. Whole-heart coronary MRA with 100% respiratory gating efficiency: self-navigated three-dimensional retrospective image-based motion correction (TRIM). Magn Reson Med. 2014; 71:67–74. [PubMed: 23401157]
14. Piccini D, Monney P, Sierro C, et al. Respiratory self-navigated post-contrast whole-heart coronary MR angiography: initial experience in patients. Radiology. 2014; 270:378–386. [PubMed: 24471387]
15. Piccini D, Bonanno G, Ginami G, Littmann A, Zenge MO, Stuber M. Is there an optimal respiratory reference position for self-navigated whole-heart coronary MR angiography? J Magn Reson Imaging. 2016; 43:426–433. [PubMed: 26174582]
16. Renker M, Varga-Szemes A, Schoepf UJ, et al. A non-contrast self-navigated 3-dimensional MR technique for aortic root and vascular access route assessment in the context of transcatheter aortic valve replacement: proof of concept. Eur Radiol. 2016; 26:951–958. [PubMed: 26188657]
17. Monney P, Piccini D, Rutz T, et al. Single centre experience of the application of self navigated 3D whole heart cardiovascular magnetic resonance for the assessment of cardiac anatomy in congenital heart disease. J Cardiovasc Magn Reson. 2015; 17:55. [PubMed: 26156377]
18. Manke D, Nehrke K, Bornert P, Rosch P, Dossel O. Respiratory motion in coronary magnetic resonance angiography: a comparison of different motion models. J Magn Reson Imaging. 2002; 15:661–671. [PubMed: 12112516]
19. Prieto C, Doneva M, Usman M, Henningsson M, Greil G, Schaeffter T, Botnar RM. Highly efficient respiratory motion compensated free-breathing coronary mra using golden-step Cartesian acquisition. J Magn Reson Imaging. 2015; 41:738–746. [PubMed: 24573992]
20. Bonanno G, Puy G, Wiaux Y, van Heeswijk RB, Piccini D, Stuber M. Self-navigation with compressed sensing for 2D translational motion correction in free-breathing coronary MRI: a feasibility study. PloS One. 2014; 9:e105523. [PubMed: 25171369]
21. Lustig M, Donoho D, Pauly JM. Sparse MRI: the application of compressed sensing for rapid MR imaging. Magn Reson Med. 2007; 58:1182–1195. [PubMed: 17969013]
22. Otazo R, Kim D, Axel L, Sodickson DK. Combination of compressed sensing and parallel imaging for highly accelerated first-pass cardiac perfusion MRI. Magn Reson Med. 2010; 64:767–776. [PubMed: 20535813]
23. Feng L, Axel L, Chandarana H, Block KT, Sodickson DK, Otazo R. XD-GRASP: golden-angle radial MRI with reconstruction of extra motion-state dimensions using compressed sensing. Magn Reson Med. 2016; 75:775–788. [PubMed: 25809847]
24. Piccini D, Littmann A, Nielles-Vallespin S, Zenge MO. Spiral phyllotaxis: the natural way to construct a 3D radial trajectory in MRI. Magn Reson Med. 2011; 66:1049–1056. [PubMed: 21469185]
25. Bonanno, G., Piccini, D., Maréchal, B., Zenge, MO., Stuber, MA. New Binning Approach for 3D Motion Corrected Self-Navigated Whole-Heart Coronary MRA Using Independent Component Analysis of Individual Coils. In Proceedings of the 22nd Annual Meeting of ISMRM; Milan, Italy. 2014. p. 936

26. Larson AC, White RD, Laub G, McVeigh ER, Li D, Simonetti OP. Selfgated cardiac cine MRI. Magn Reson Med. 2004; 51:93–102. [PubMed: 14705049]
27. Hyvarinen A. Fast and robust fixed-point algorithms for independent component analysis. IEEE Trans Neural Netw. 1999; 10:626–634. [PubMed: 18252563]
28. Buehrer M, Curcic J, Boesiger P, Kozerke S. Prospective self-gating for simultaneous compensation of cardiac and respiratory motion. Magn Reson Med. 2008; 60:683–690. [PubMed: 18727084]
29. Feng L, Sirchai MB, Lim RP, Harrison A, King W, Adluru G, Dibella EVR, Sodickson DK, Otazo R, Kim D. Highly accelerated real-time cardiac cine MRI using k-t SPARSE-SENSE. Magn Reson Med. 2013; 70:64–74. [PubMed: 22887290]
30. Walsh DO, Gmitro AF, Marcellin MW. Adaptive reconstruction of phased array MR imagery. Magn Reson Med. 2000; 43:682–690. [PubMed: 10800033]
31. Knoll, F., Schwarzl, A., Diwoky, C., Sodickson, DK. gpuNUFFT - An Open Source GPU Library for 3D Regridding with Direct MATLAB Interface. In Proceedings of the 22nd Annual Meeting of ISMRM; Milan, Italy. 2014. p. 4297
32. Austen WG, Edwards JE, Frye RL, Gensini GG, Gott VL, Griffith LS, McGoon DC, Murphy ML, Roe BB. A reporting system on patients evaluated for coronary artery disease. Report of the Ad Hoc Committee for Grading of Coronary Artery Disease, Council on Cardiovascular Surgery, American Heart Association. Circulation. 1975; 51:5–40. [PubMed: 1116248]
33. Etienne A, Botnar RM, Van Muiswinkel AM, Boesiger P, Manning WJ, Stuber M. "Soap-Bubble" visualization and quantitative analysis of 3D coronary magnetic resonance angiograms. Magn Reson Med. 2002; 48:658–666. [PubMed: 12353283]
34. McConnell MV, Khasgiwala VC, Savord BJ, Chen MH, Chuang ML, Edelman RR, Manning WJ. Comparison of respiratory suppression methods and navigator locations for MR coronary angiography. Am J Roentgenol. 1997; 168:1369–1375. [PubMed: 9129447]
35. Schmidt JF, Buehrer M, Boesiger P, Kozerke S. Nonrigid retrospective respiratory motion correction in whole-heart coronary MRA. Magn Reson Med. 2011; 66:1541–1549. [PubMed: 21604297]
36. Aitken AP, Henningsson M, Botnar RM, Schaeffter T, Prieto C. 100% Efficient three-dimensional coronary MR angiography with two-dimensional beat-to-beat translational and bin-to-bin affine motion correction. Magn Reson Med. 2015; 74:756–764. [PubMed: 25236813]
37. Ingle RR, Wu HH, Addy NO, Cheng JY, Yang PC, Hu BS, Nishimura DG. Nonrigid autofocus motion correction for coronary MR angiography with a 3D cones trajectory. Magn Reson Med. 2014; 72:347–361. [PubMed: 24006292]
38. Ginami G, Bonanno G, Schwitter J, Stuber M, Piccini D. An iterative approach to respiratory self-navigated whole-heart coronary MRA significantly improves image quality in a preliminary patient study. Magn Reson Med. 2016; 75:1594–1604. [PubMed: 25960337]
39. Akcakaya M, Basha TA, Chan RH, Manning WJ, Nezafat R. Accelerated isotropic sub-millimeter whole-heart coronary MRI: compressed sensing versus parallel imaging. Magn Reson Med. 2014; 71:815–822. [PubMed: 23440946]
40. Akcakaya M, Nam S, Hu P, Moghari MH, Ngo LH, Tarokh V, Manning WJ, Nezafat R. Compressed sensing with wavelet domain dependencies for coronary MRI: a retrospective study. IEEE Trans Med Imaging. 2011; 30:1090–1099. [PubMed: 21536523]
41. Moghari MH, Akcakaya M, O'Connor A, et al. Compressed-sensing motion compensation (CosMo): a joint prospective-retrospective respiratory navigator for coronary MRI. Magn Reson Med. 2011; 66:1674–1681. [PubMed: 21671266]
42. Forman C, Piccini D, Grimm R, Hutter J, Hornegger J, Zenge MO. High-resolution 3D whole-heart coronary MRA: a study on the combination of data acquisition in multiple breath-holds and 1D residual respiratory motion compensation. Magn Reson Mater Phy. 2014; 27:435–443.
43. Forman C, Piccini D, Grimm R, Hutter J, Hornegger J, Zenge MO. Reduction of respiratory motion artifacts for free-breathing whole-heart coronary MRA by weighted iterative reconstruction. Magn Reson Med. 2014; 73:1885–1895. [PubMed: 24912763]

44. Pang J, Sharif B, Fan Z, Bi X, Arsanjani R, Berman DS, Li D. ECG and navigator-free four-dimensional whole-heart coronary MRA for simultaneous visualization of cardiac anatomy and function. Magn Reson Med. 2014; 72:1208–1217. [PubMed: 25216287]

45. Coppo S, Piccini D, Bonanno G, Chaptinel J, Vincenti G, Feliciano H, van Heeswijk RB, Schwitter J, Stuber M. Free-running 4D whole-heart self-navigated golden angle MRI: initial results. Magn Reson Med. 2015; 74:1306–1316. [PubMed: 25376772]

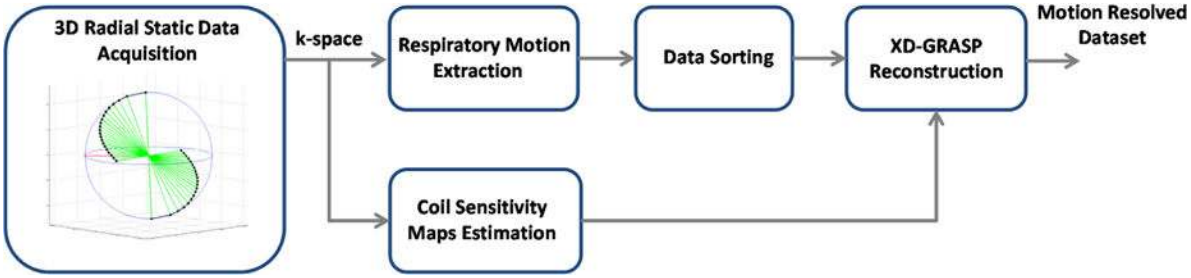

FIG. 1.

Schematic representation of the proposed acquisition/reconstruction pipeline. The flow chart shows how the radial k-space lines of the whole heart coronary MRA datasets are acquired with a 3D radial acquisition scheme, as opposed to the 2D radial stack-of-stars scheme proposed in the original publication. The acquired static data are first used for respiratory motion extraction and then consequently binned into distinct respiratory phases via the data sorting procedure. The sorted data are then fed into the XD-GRASP sparse iterative reconstruction algorithm to generate the final respiratory motion-resolved dataset. Coil sensitivity maps are also directly extracted from the radial acquisition and subsequently used in the iterative reconstruction.

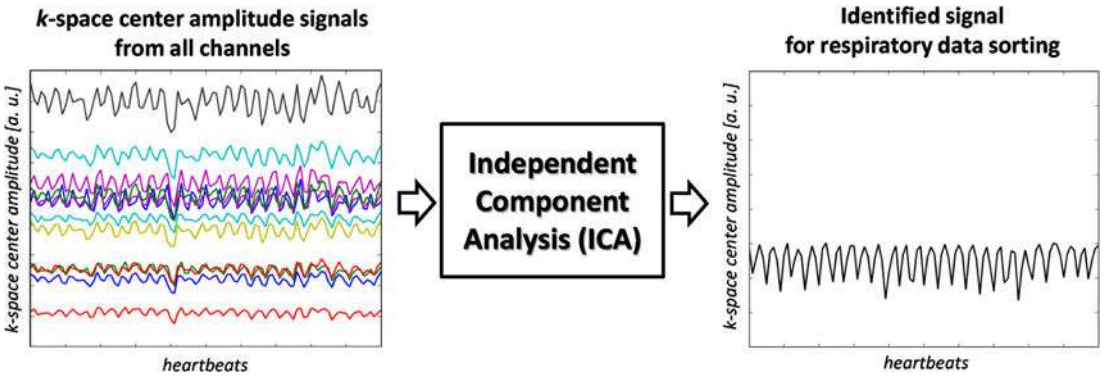

FIG. 2.

Procedure for respiratory motion detection. First, separate components of the KCA signal are extracted from the SI readouts for each receiver coil element (left). Subsequently, independent component analysis is performed on all KCA signals to identify different independent components (center). The component with highest amplitude in the frequency range of respiration (right, black line) is then selected and used as the respiratory motion signal for data sorting into respiratory bins.

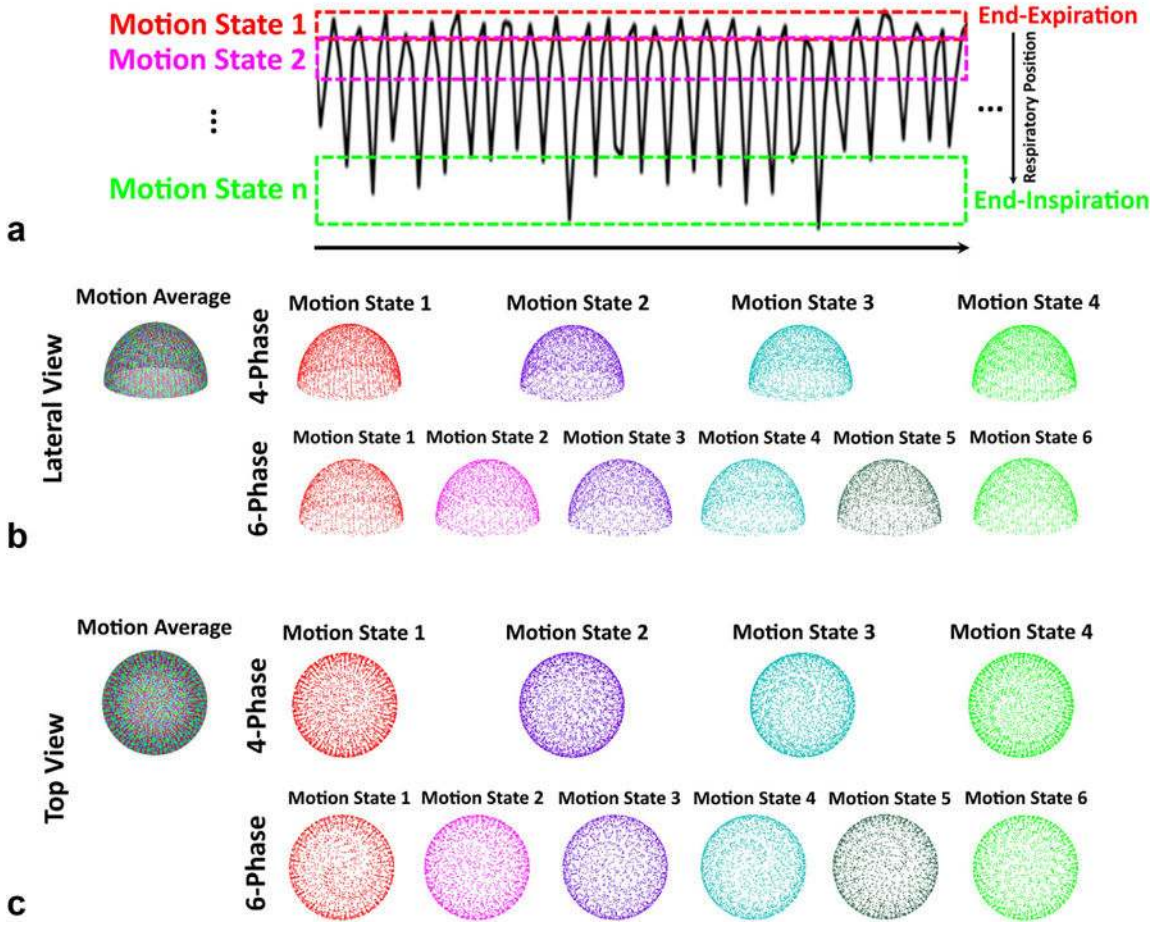

FIG. 3.

Data sorting procedure for XD-GRASP reconstruction. (**a**) The whole heart coronary MRA dataset acquired using the phyllotaxis 3D radial trajectory can be binned into any number (n) of respiratory phases, spanning from end-expiration (top) to end-inspiration (bottom), using the motion signal detected. Each dot represents the origin (on the top half of k-space) of a linear readout going through the center of k-space. The binning procedure is then performed so that the number of spokes grouped in each respiratory phase is equal, therefore leading to different bin widths. (**b**, **c**) Due to the golden angle acquisition scheme, approximately uniform coverage of k-space with distinct sampling patterns in each phase is always achieved. Two examples of data binning with four (b) and six (c) separate phases are shown.

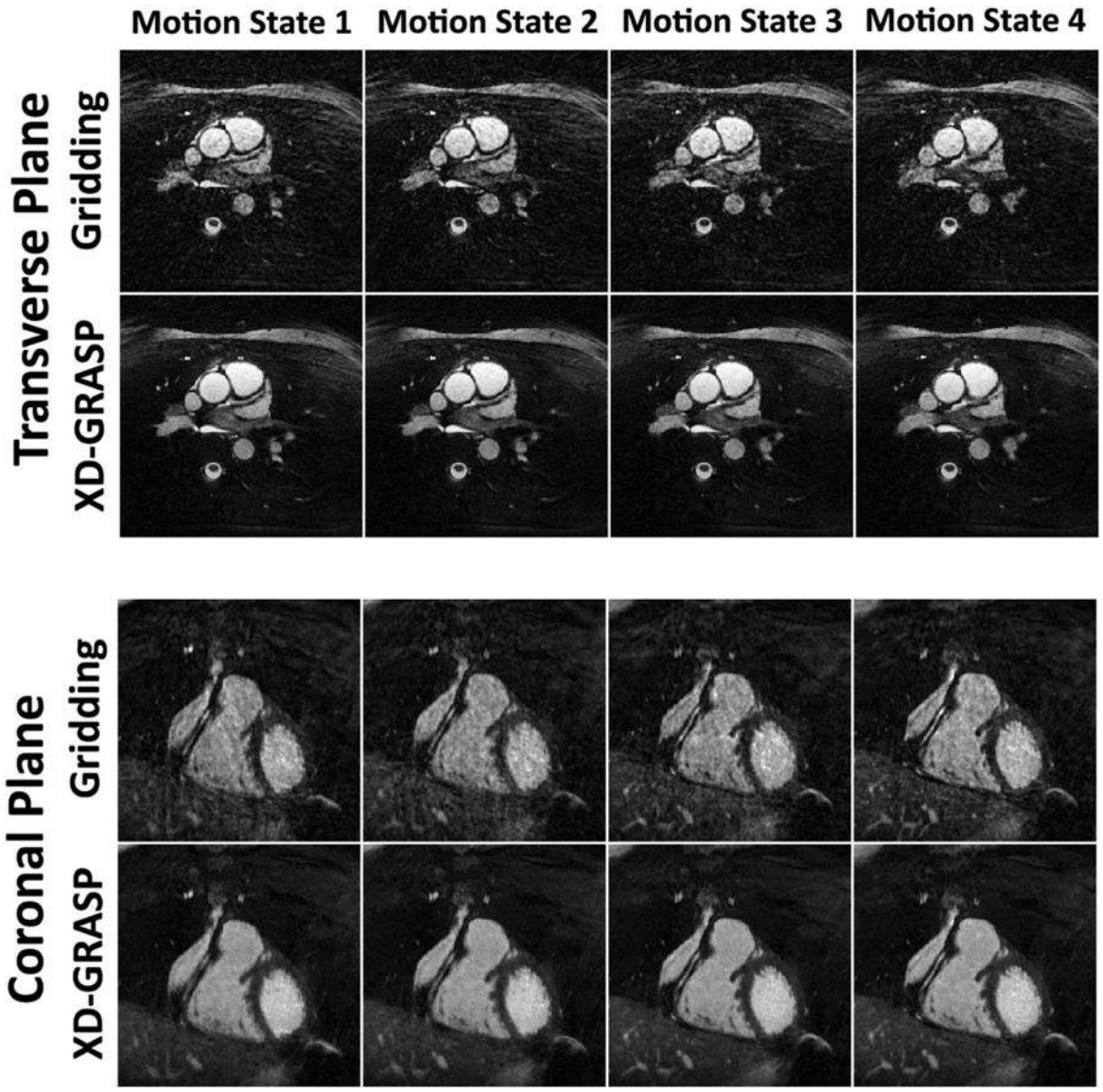

FIG. 4.

Example from one representative healthy adult volunteer comparing conventional sensitivity-weighted multicoil gridding reconstruction with the four-phase XD-GRASP reconstruction. All reconstructed phases are shown in an axial plane (top) and a coronal plane (bottom). Respiratory motion is resolved by sorting the data into different motion states, while the streaking artifacts due to undersampling are effectively removed in the XD-GRASP reconstruction.

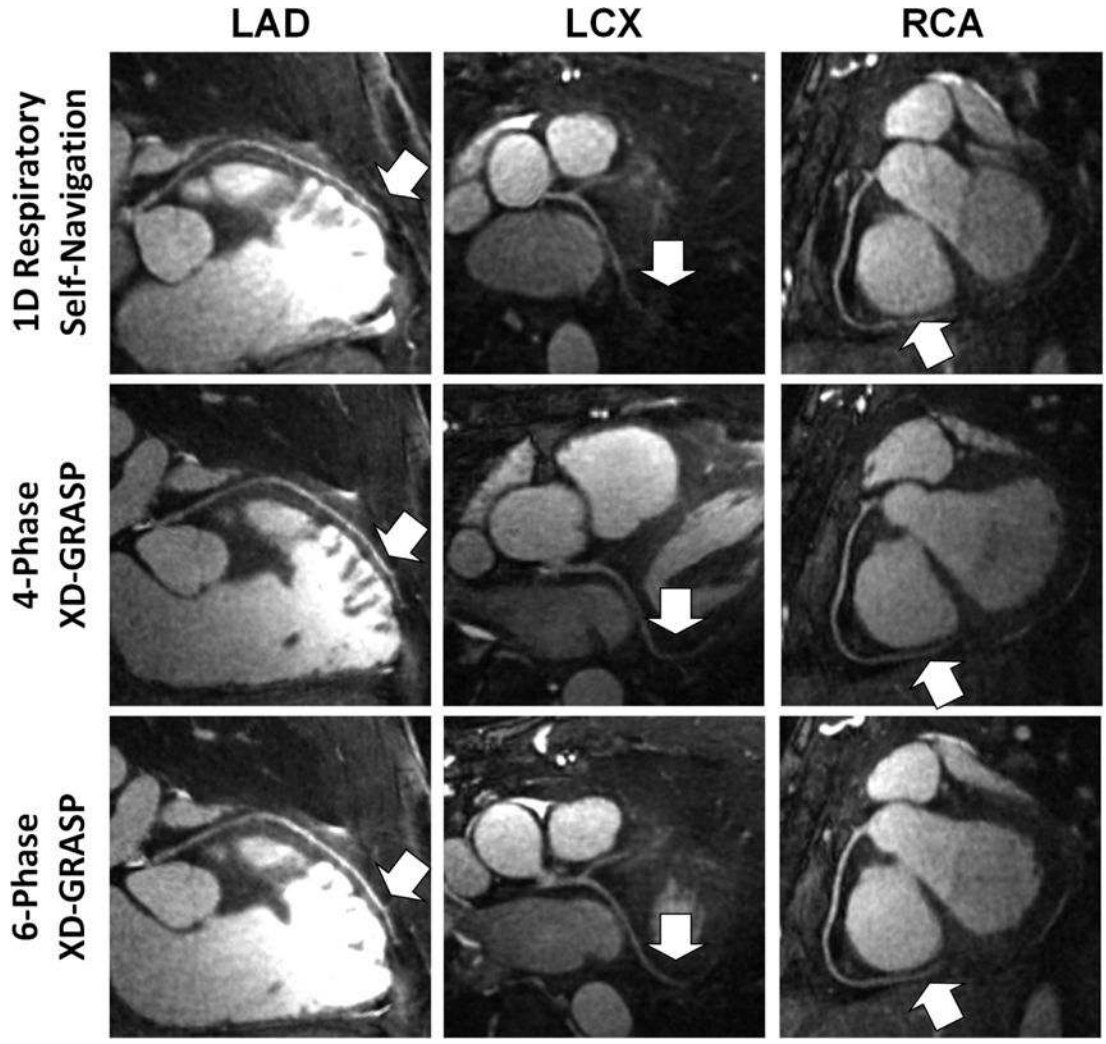

FIG. 5.

Examples of multiplanar reformatted coronary arteries from one representative healthy adult volunteer. Although respiratory self-navigated reconstruction with 1D motion correction could achieve high image quality (top row), a clear improvement in sharpness as well as visible vessel length (arrows) can be noticed in both four-phase (middle row) and six-phase (bottom row) XD-GRASP reconstructions.

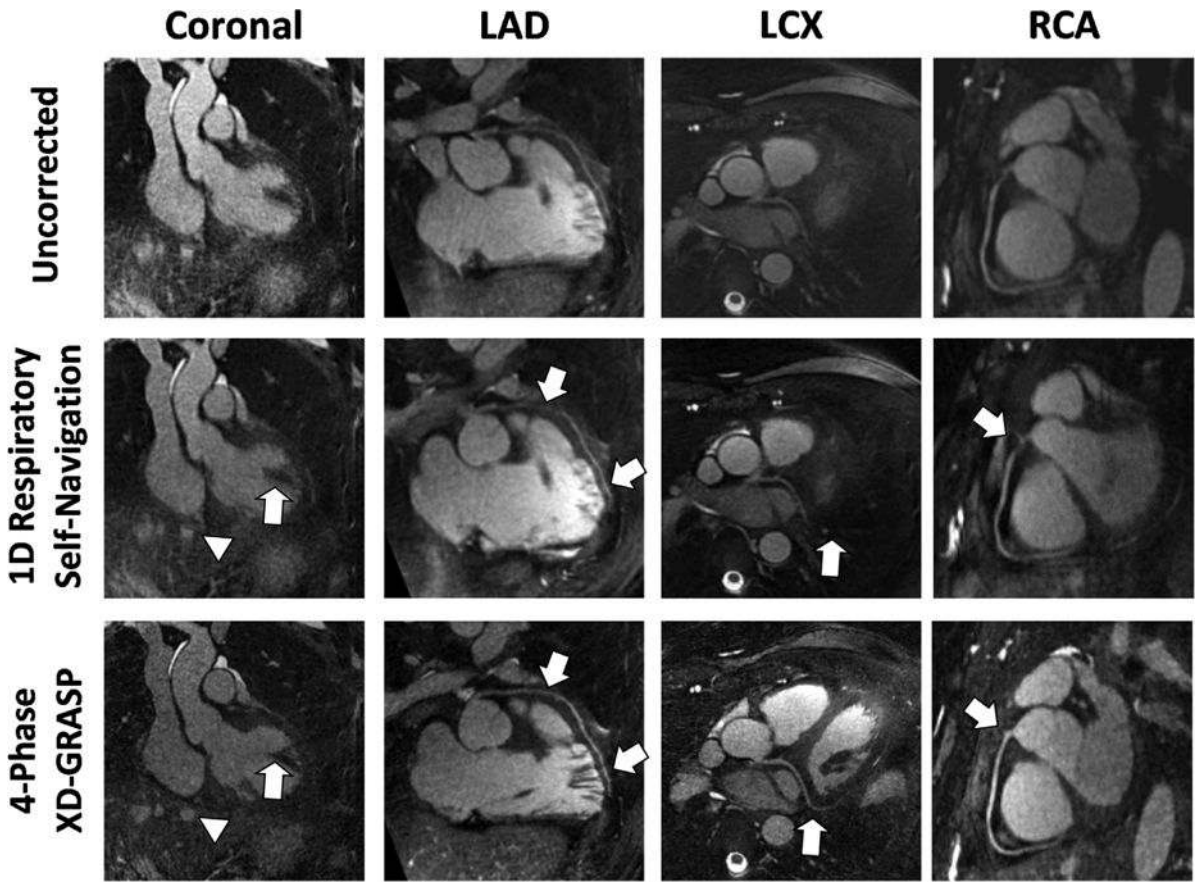

FIG. 6.

Example of a selected healthy adult volunteer dataset in which 1D respiratory self-navigation did not lead to diagnostic image quality. Although a clear improvement can be noticed from the uncorrected reconstruction to 1D respiratory self-navigation, the coronal view still shows strong residual blurring after conventional respiratory motion correction. Only the proximal segments of LAD and LCX are visible, whereas the RCA, although visible, was not scored with full diagnostic quality in the mid- and distal segments. By contrast, the dataset provided by the XD-GRASP reconstruction shows sharp and well-defined margins of a papillary muscle in the left ventricle and of the liver on the coronal view (arrowheads). All coronary arteries were better depicted, and increased vessel length could be seen with XD-GRASP reconstruction. Coronary segments graded as visible but nondiagnostic in the 1D respiratory self-navigation were considered diagnostic with the proposed XD-GRASP methodology (arrows).

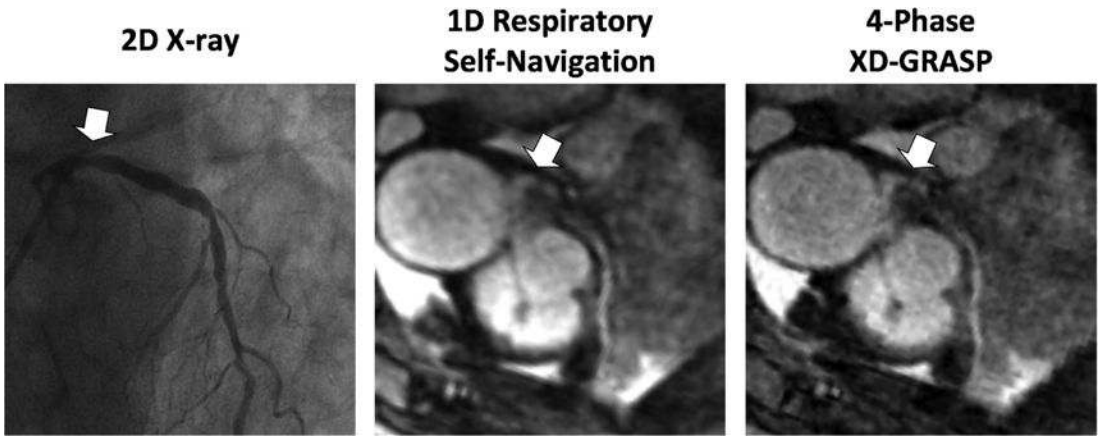

FIG. 7.

Sample images from a selected patient dataset. Both 1D respiratory self-navigation and the four-phase XD-GRASP reconstruction can be compared directly with the standard 2D X-ray angiogram. The X-ray angiogram shows a significant stenosis of the proximal LAD, which is also well visualized in the corresponding self-navigated dataset (arrows). The four-phase XD-GRASP reconstruction does not affect depiction of the stenosis (arrow), whereas the vessel itself appears to be even sharper. The signal void present on MR images distal to the stenosis is caused by the presence of a coronary stent in the proximal LCX.

Table 1

Quality Grading and Quantitative Assessment

			XD-GRASP	
Coronary Segment	**Measured Parameter**	**1D Self-Navigation**	**Four-Phase**	**Six-Phase**
LM	Image quality grading	1.8 ± 0.8	2.0 ± 0.5	2.1 ± 0.5
	Sharpness (%)	48.4 ± 7.7	55.1 ± 7.7[a]	49.1 ± 8.5
LAD (proximal)	Image quality grading	1.5 ± 0.8	1.9 ± 0.5	2.0 ± 0.6
	Sharpness (%)	37.3 ± 8.6	41.9 ± 8.1[a]	40.2 ± 7.7
LAD (mid)	Image quality grading	1.0 ± 0.8	1.5 ± 0.4[a]	1.5 ± 0.6[a]
	Sharpness (%)	34.9 ± 10.2	40.8 ± 9.1[a]	38.7 ± 8.7
LAD (distal)	Image quality grading	0.8 ± 0.6	1.1 ± 0.6	1.2 ± 0.8
LM+LAD	Length (cm)	11.7 ± 3.2	13.2 ± 3.1[a]	12.8 ± 3.1[a]
LCX (proximal)	Image quality grading	1.1 ± 0.7	1.0 ± 0.5	1.0 ± 0.5
	Sharpness (%)	43.2 ± 9.3	46.3 ± 12.9	48.7 ± 7.9
RCA (proximal)	Image quality grading	1.9 ± 0.7	2.2 ± 0.4	2.3 ± 0.5
	Sharpness (%)	46.9 ± 11.0	53.2 ± 5.3	52.5 ± 5.6
RCA (mid)	Image quality grading	1.7 ± 0.6	2.0 ± 0.4	2.2 ± 0.7[a]
	Sharpness (%)	42.9 ± 10.4	49.8 ± 6.2[a]	49.9 ± 7.5[a]
RCA (distal)	Image quality grading	1.2 ± 0.8	1.5 ± 0.4	1.7 ± 0.7[a]
RCA	Length (cm)	11.2 ± 2.5	12.1 ± 1.6	11.7 ± 3.1

All values are expressed as the mean ± standard deviation of the image quality grades, vessel sharpness, and length for the 11 volunteers and using 1D respiratory self-navigation compared with the proposed respiratory-resolved XD-GRASP reconstruction. The image quality grading system was as follows: 0 = not visible, 1 = markedly blurred, 2 = moderately blurred, 3 = mildly blurred, and 4 = sharply defined.

Abbreviations: LAD, left anterior descending artery; LCX, left circumflex artery; LM, left main stem; RCA, right coronary artery; XD-GRASP, extradimensional golden-angle radial sparse parallel MRI.

[a]Indicates statistical significance compared with 1D respiratory self-navigation.

Table 2

Diagnostic Quality Grading

		XD-GRASP	
Coronary Segment	**1D Respiratory Self-Navigation**	**Four-Phase**	**Six-Phase**
LM	1.8 ± 0.4	2.0 ± 0.0	2.0 ± 0.0
LAD (proximal)	1.6 ± 0.5	2.0 ± 0.0	1.7 ± 0.5
LAD (mid)	1.3 ± 0.6	1.4 ± 0.5	1.5 ± 0.5
LAD (distal)	0.9 ± 0.5	1.3 ± 0.5	1.3 ± 0.5
LCX (proximal)	1.4 ± 0.7	1.4 ± 0.7	1.4 ± 0.7
RCA (proximal)	1.8 ± 0.4	2.0 ± 0.0	2.0 ± 0.0
RCA (mid)	1.3 ± 0.5	1.7 ± 0.5	1.5 ± 0.5
RCA (distal)	1.4 ± 0.7	1.7 ± 0.5	1.6 ± 0.5
Total diagnostic segments	41/88 (47%)	61/88 (70%)[a]	56/88 (63%)[a]

All values are expressed as mean ± standard deviation for diagnostic quality grades for the 11 volunteers, using 1D respiratory self-navigation compared with the proposed XD-GRASP reconstruction. A clear improvement was seen in the datasets where respiratory-resolved XD-GRASP reconstruction was applied. The diagnostic quality grading system was as follows: 0 = not visible, 1 = visible but nondiagnostic, and 2 = visible and diagnostic.

Abbreviations: LAD, left anterior descending artery; LCX, left circumflex artery; LM, left main stem; RCA, right coronary artery; XD-GRASP, extradimensional golden-angle radial sparse parallel MRI.

[a]Indicates statistical significance compared with 1D respiratory self-navigation.